Supporting Information

Sylantyev et al. 10.1073/pnas.1211204110

SI Methods

Chemicals. Thapsigargin, ryanodine, strychnine, TTX, WIN55,212-2, Δ^9tetrahydrocannabinol (Δ^9THC), T1117, and CGP 55845 were purchased from Tocris Cookson; (2R)-amino-5-phosphonovaleric acid (D-APV), QX-314, (S)-α-methyl-4-carboxyphenylglycine (MCPG), cannabidiol, and picrotoxin were purchased from Ascent Scientifi; other chemicals were purchased from Sigma-Aldrich. L-α-Lysophosphatidylinositol sodium salt from soybean was obtained from Sigma (product no. 62966), with the full structural formula available online at Merk Millipore catalog No 440153–1MG, and composition and properties are as follows: 2.1–5.3% (wt/wt) sodium, ≥55% palmitic acid, ≤20% stearic acid, ≤5% oleic acid, ≤5% linolenic acid, ≤15% linoleic acid; ≥95% purity, solubility (turbidity) clear at 25 mg plus 1 mL of $CHCl_3$:MeOH:H_2O (70:27:3).

Preparation. Acute hippocampal slices 350 μm thick were obtained from 3- to 4-wk-old rats, 5- to 6-wk-old wild-type mice (CB57BL), and age-matched G protein-coupled receptor (GPR)55 knockout mice ($Gpr55^{tm1Lex}$, involves the following: 129S/SvEvBrd × C57BL/6J) and CB_1 knockout mice (ABH-background species, supplied by David Baker; original supply by Catherine Leden), as specified, in full compliance with national guidelines on animal experimentation. Our initial observations were obtained in rats, and we then expanded our studies by using knockouts and wild-type controls. Slices were prepared in an ice-cold slicing solution containing 60 mM NaCl, 105 mM sucrose, 2.5 mM KCl, 7 mM $MgCl_2$, 1.25 mM NaH_2PO_4, 0.5 mM $CaCl_2$, 6.5 mM ascorbic acid, 3 mM sodium pyruvate, and 8 mM glucose (osmolarity 300–310 mOsM), stored in the slicing solution at 34 °C for 15 min before being transferred to an interface chamber for storage in an extracellular storage solution containing 119 mM NaCl, 2.5 mM KCl, 1.3 mM $MgSO_4$, 1 mM NaH_2PO_4, 26 mM $NaHCO_3$, 2 mM $CaCl_2$, and 25 mM glucose (osmolarity adjusted to 295–305 mOsM with glucose). All solutions were continuously bubbled with 95% O_2/5% CO_2. Slices were allowed to rest for at least 60 min before recordings started.

For experiments in cultures, hippocampal neurons were isolated from postnatal days 0–2 rat pups and cultured in Neurobasal-based medium, as described (1). All experiments were conducted at near-physiological temperature (~34 °C) 20–24 d after plating to match the age of the acute slice preparations. Neurons were selected for recording if they were close to an empty patch (devoid of any astroglial elements) on the coverslip, and only those axonal boutons were included where the axon passed over the empty patch and had no surrounding structures except for the postsynaptic dendrite. Imaging settings were similar to those in acute slice experiments (λ_x^{2P} ~800 nm) to ensure similarity of imaging conditions.

Electrophysiology. Slices were transferred to the submersion-type recording chamber and superperfused, at 34 °C, with artificial cerebrospinal fluid saturated with 95% O_2/5% CO_2 containing 125 mM NaCl, 2.5 mM KCl, 1.25 mM NaH_2PO_4, 26 mM $NaHCO_3$, and 25 mM glucose (pH 7.4; osmolarity 295–305 mOsM) in the presence of 1.3 mM Mg^{2+} and 2.0 mM Ca^{2+}. In experiments where cell depolarization could induce spiking, we used a standard Cs-based intracellular solution: 120 mM Cs-gluconate, 10 mM CsCl, 10 mM KOH-Hepes, 10 mM BAPTA, 8 mM NaCl, 5 mM QX-314, and 2 mM Mg-ATP, 0.3 mM GTP (pH adjusted to 7.2 with KOH, osmolarity 290–295 mOsm). To buffer postsynaptic Ca^{2+} with high total concentration of BAPTA (100 mM), we used Cs-based solution including 90 mM tetracesium-BAPTA, 10 mM BAPTA, 10 mM KOH-Hepes, 8 mM NaCl, 5 mM QX-314, 2 mM Mg-ATP, and 0.3 mM GTP.

Where indicated, receptor agonists and antagonists purchased from Tocris Cookson or Sigma were added to the artificial cerebrospinal fluid at the following concentrations: 1 μM TTX, 10 μM 2,3-dihydroxy-6-nitro-7-sulfamoyl-benzo[f]quinoxaline-2,3-dione (NBQX), 50 μM APV, 100 μM Picrotoxin, 200 or 500 μM S-MCPG, 1 μM strychnine, 40 μM MK801, and 4 μM lysophosphatidylinositol. Vehicles of dH_2O or DMSO were used, and the DMSO concentration never exceeded 0.01% [in the experiment with (-)-Xestospongin C the DMSO concentration in a vehicle solution applied locally was 0.25%; vehicle controls were recorded]. In experiments where presynaptic Ca^{2+} transients were recorded, CA3 pyramidal cells were recorded from in whole-cell mode by using 3–3.5MΩ pipettes containing 135 mM KCH_3O_3S, 10 mM Hepes, 10 mM disodium phosphocreatine, 4 mM $MgCl_2$, 4 mM Na_2ATP, 0.4 mM Na_3GTP (pH adjusted to 7.2 with KOH, osmolarity 290–295 mOsm) and also fluorophores as indicated. For postsynaptic recordings, the same solution was used with the inclusion of 5 mM QX-314. In recordings of miniature miniature excitatory postsynaptic currents (mEPSCs) (voltage-clamp) and field excitatory postsynaptic potentials (fEPSPs) in area CA1, AMPA receptor components were isolated by adding of 0.1 μM CGP 55845, 100 μM D-APV, 200 μM (S-form) or 500 μM MCPG (alternatively, mGluRs were blocked 500 nM MPEP + 100 μM LY367385 + 50 nM LY341495), 1 μM strychnine, and 100 μM picrotoxin (experiments with mEPSCs also included 1 μM TTX in the ACSF); correspondingly, NMDA receptor currents were isolated by adding 10 μM NBQX (instead of D-APV) and recorded at +40 mV. Schaffer collaterals were stimulated with the bipolar tungsten electrode. In experiments on fEPSPs glass recording electrode (1–2 MOhm resistance) was filled with 2 M solution of NaCl and placed in stratum radiatum, the stimulus intensity was set at ~70% of that triggering population spikes, stimuli were applied every 15 s. Posttetanic potentiation (PBP) was induced by a brief train of high-frequency stimulation (10 pulses at 100 Hz); in rat groups, three trains (60 s apart) were applied to achieve stable responses; in mouse groups, one train was applied. The slope of fEPSPs was monitored for a subsequent 30–50 min. Electrophysiological recordings were carried out by using a set of remotely controlled micromanipulators (Scientifica UK) and a Multiclamp 700A or 700B amplifier (Molecular Devices). Signals were digitized at 10 kHz and stored for off-line analysis by using pClamp10 software (Molecular Devices) or WinWCP V4.1.5 (John Dempster, University of Strathcyde). As a general rule, we used field recordings (fEPSPs) to have a bulk measure of synaptic responses while leaving postsynaptic cells intact, whereas whole-cell recordings were required to document responses at individual synapses, to manipulate intracellular solution, and to carry our Ca^{2+} imaging experiments.

Mouse Species. The GPR55 KO animals ($Gpr55^{tm1Lex}$/$Gpr55^{tm1Lex}$; 4- to 5-wk-old; genetic background involves 129S/SvEvBrd × C57BL/6J) were supplied by Harlan Laboratories and University of Aberdeen or Queen Mary University of London; the wild-type mice were C57BL/6J; CB_1 KO mice (ABH background) were kindly supplied by David Baker and Catherine Ledent. KO mice were fully congenic over 11 generations of backcrossing before intercross.

Two-Photon Excitation Imaging and Uncaging. We used a Radiance 2100 imaging system (Zeiss–Bio-Rad) optically linked to two femtosecond-pulse lasers MaiTai (SpectraPhysics-Newport) and integrated with patch-clamp electrophysiology (2, 3). For morphological tracing purposes, cell processes were visualized at the maximal optical resolution as a series of individual 3D stacks (10- to 15-μm-deep each) in the Alexa emission channel (540LP/700SP filter; $\lambda_x{}^2{}_p$ = 800 nm), collected in image frame mode (512 × 512 pixels, 8-bit) at 0.5- to 1-μm steps. For illustration purposes, individual stacks were averaged by using ImageJ routines (ImageJ; National Institutes of Health).

For presynaptic Ca^{2+} imaging, CA3 pyramidal cells were routinely patched in CA3a most proximal to CA2. Once in whole-cell mode, pyramidal cells were visually inspected and accepted as CA3 pyramidal cells if dendrites branched close to the cell body and distinct thorny excrescences were visible, indicating mossy fiber innervation. If accepted, 45–60 min was allowed for Alexa 594 to equilibrate across the axonal arbor. Following this period, axons were traced into the CA1 region (up to 500 μm, inside stratum radiatum) from the cell body where discrete boutons were identified by criteria previously demonstrated to reliably match synaptophysin labeled punctae (4). For fast imaging of action potential mediated Ca^{2+} transients, line scans were taken with a sampling frequency of 500 Hz and a pixel size of ∼40 nm. For time-lapse imaging of store-mediated Ca^{2+} transients, three to four sets of 190 frames of Alexa 594 and Fluo4 (or OGB-1) fluorescence image frames were recorded at a rate of 1 Hz (256 × 256 pixels, ∼80 nm pixel size, duration 3.1 min, 15 s interval between acquisitions) unless otherwise indicated.

For postsynaptic imaging of Ca^{2+} responses in CA1 pyramidal cell dendrites and spines, time-lapse imaging and line scans with appropriate durations were used as described in the main text. To record synaptically evoked Ca^{2+} responses, a monopolar glass stimulating electrode filled with artificial cerebrospinal fluid was placed 15–30 μm from the dendritic branch targeted. To identify active synapses relatively fast (10 Hz), frame scans of the local dendrites were viewed while three 100-μs square pulses of 2–10 V were delivered with a 25-ms interstimulus interval by using a constant voltage isolated stimulator (model DS2A-mkII; Digitimer). This protocol was repeated until a Ca^{2+} response confined to a spine head was observed, then 400-ms line scans of the active spine were then recorded while a dual stimulus (50-ms interstimulus interval) was delivered. Scans were repeated once every 30 s with a minimum of 15 trials in each condition was used to assess the release probability imaged synapse. Astrocytes were identified, patched in whole-cell mode and imaged in two-photon excitation mode as described (5).

IP_3 uncaging evoked Ca^{2+} transients were recorded as described (3); in brief, caged IP_3 [D-myo-inositol 1,4,5-triphosphate, P4(5)-(1-(2-nitrophenyl)ethyl) ester, Tris(triethylammonium) salt, 400 μM; Invitrogen] was added to the intracellular solution with the Ca^{2+} indicator Fluo 4 and the morphological tracer Alexa 594 (both excited in the main imaging channel at $\lambda_x{}^{2P}$ = 800 nm). Once the indicators equilibrated (20–30 mins), the dendrite of interest was traced from the soma and the IP3 cage was excited, in two-photon mode, at $\lambda_u{}^{2P}$ = 720 nm (10 5-ms pulses 25 ms apart) while recording the local Ca^{2+} signal by a line scan lasting 5 s.

Fluorescent Ca^{2+} responses evoked either in axonal boutons or in dendritic spines were routinely imaged in the Ca^{2+} sensitive (green) emission channel (515/30 filter, with indicators Fluo-4 or OGB-1) in line scan mode (scanning rate as specified Hertz) and corrected for focus fluctuations in the Alexa (red) channel, as detailed (4, 6, 7) and illustrated in the figures. Briefly, Ca^{2+} signals were routinely documented as $\Delta G/R$, where $\Delta G = G - G_0$ stands for the fluorescence signal in the green channel G with the baseline fluorescence G_0 (averaged over the baseline time window) subtracted, and R stands for the Alexa fluorescence in the red channel (corrected for photobleaching, if any). Because the success rate of tracing and imaging individual dendritic spines or axonal boutons was relatively low, each such experiment normally represented one cell–one slice–one animal.

Immunohistochemistry. ***Preparation and confocal microscopy.*** Acute hippocampal slices were prepared for immunohistochemistry by using techniques adapted from refs. 8 and 9. In brief, 4-wk-old wild-type or GPR55 knockout mouse brains were fixed overnight in 4% paraformaldehyde in PBS. The next morning, 50-μm-thick transverse brain slices were cut by using a Leica VT1000S microtome. After cutting, slices were washed in PBS then incubated for 5 h at 37 °C in PBS containing 10% goat serum, 1% BSA, and 0.5% Triton X-100 to block nonspecific binding and permeabilize the slices. Slices were then washed in PBS and incubated overnight at room temperature with the primary anti-GPR55 antibody (provided by Ken Mackie) and diluted at 1:500 with the primary anti-vesicle glutamate transporter 1 (VGLUT1) antibody (Chemicon) diluted at 1:1000 in PBS containing 10% goat serum and 1% BSA. After this procedure, slices were washed with PBS five times (1, 10, 10, 10, and 10 mins) then incubated for 4 h with Alexa-conjugated goat anti-rabbit (Alexa 488 to label GPR55) and goat anti-guinea pig (Alexa 568 to label VGLUT1) secondary antibodies (Invitrogen) diluted at 1:500 in PBS containing 10% goat serum and 1% BSA. Slices were then washed in PBS five times (1, 10, 10, 10, and 10 mins) then mounted and coversliped by using Vectorshield (hard set). Slides were then transferred to the stage of the confocal microscope used in imaging experiments, and using 488- nm and 568-nm Krypton laser lines for excitation of the Alexa 488 and 568, respectively, fluorescence emitted from the secondary antibodies were collected and filtered at 515 ± 30 nm (Alexa 488) and 600 ± 40 nm (Alexa 568). Once the optimal confocal aperture, laser power and gain settings were achieved these settings remained constant across all samples examined.

Data analyses. For GPR55-only staining analyses, we used a symmetrical two-factor design with equally weighted samples taken from five wild-type and five GPR55 knockout animals, with three slices processed for each animal and three quasirandomly selected regions of interest (ROIs, ∼66 × 66 μm each) sampled in stratum radiatum and stratum pyramidale of each slice (Fig. 4*A*). The data were arranged for two-way ANOVA, with two fixed factors (gene and hippocampal region) and one random influence (animal), the latter being "nested" in the factor of hippocampal region. (Both ANOVA and straightforward paired comparisons indicated highly significant puncta staining in wild-type animals compared with GPR55 knockouts, Fig. 4 *A–C*).

Fluorescent puncta labeling was detected by using the unsupervised ImageJ threshold sliding algorithm (Gabriel Lapointe). This method: (*i*) performs binary segmentation of the image while scanning the entire range of the gray level (brightness) thresholds and (*ii*) determines the maximal number of contiguous puncta (particles) for any given threshold. This approach is largely insensitive to the average gray level, thus allowing an unbiased comparison between brighter and dimmer samples. Puncta (particle) size detection was set between 0.5 and 5 μm to exclude single-pixel noise or any potential bias from the brightness gradients; to account for all shapes of puncta, circularity was set between 0 and 1. Exactly the same settings were applied throughout all samples in a blind fashion. The extent of puncta staining was evaluated as a single parameter; the image area fraction was occupied by the detected puncta.

For GPR55-VGLUT1 colocalization analyzes, we took equally weighted samples from four wild-type animals and four GPR55 knockout animals serving as control. Samples were prepared so that in each animal (an individual staining experiment), two hippocampal slices were prepared, with three ROIs (40 × 40 μm, stratum radiatum) imaged and analyzed in each slice. Colocali-

zation pixels between the two labels (green and red channels for GPR55 and VGLUT1, respectively) were identified and counted by using an unsupervised ImageJ colocalization plugin algorithm (Pierre Bourdoncle, Institut Jacques Monod, Paris). The minimum pixel intensity ratio between the channels (bleed-through cutoff) was set at 50%, and the pixel intensity threshold was set at ~20% of the dynamic range (50/255) to remove the nonspecific background signal. To assess the degree of specific colocalization, as opposed to random coincidence in similar conditions, the colocalization test was repeated on the same pair of images but with the red image "scrambled" (normally rotated by 90°). The ratio N_c/N_s between the number of the colocalization pixels in the original GPR55-VGLUT1 image pair (N_c) and in the scrambled pair (N_s) thus provided an unbiased index of specific GPR55-VGLUT1 colocalization. Note that with all of the measures taken to suppress nonspecific signals or spurious colocalization, these numbers represent conservative indicators of colocalization rather than its absolute values. In the ANOVA design, three factors included were as follows: image scrambling (colocalization test), the animal (individual staining), and the slice factor nested within the staining factor. Similar procedures were applied in the control GPR55 KO samples, with the fluorescence background in the GPR55 channel adjusted to match that in wild-type samples.

Statistics. Group data are routinely reported as mean ± SEM, and the statistical difference between the population means was estimated by using the Student *t* test (for paired or independent samples), unless stated otherwise. The Mann–Whitney nonparametric *u* test was used when the data scatter was non-Gaussian. A two- or three-way ANOVA design was used to analyze immunohistochemistry data, as detailed above and illustrated in Fig. 4 *A* and *D*.

1. Ermolyuk YS, et al. (2012) Independent regulation of Basal neurotransmitter release efficacy by variable Ca²+ influx and bouton size at small central synapses. *PLoS Biol* 10(9):e1001396.
2. Scott R, Rusakov DA (2006) Main determinants of presynaptic Ca2+ dynamics at individual mossy fiber-CA3 pyramidal cell synapses. *J Neurosci* 26(26):7071–7081.
3. Scott R, Lalic T, Kullmann DM, Capogna M, Rusakov DA (2008) Target-cell specificity of kainate autoreceptor and Ca2+-store-dependent short-term plasticity at hippocampal mossy fiber synapses. *J Neurosci* 28(49):13139–13149.
4. Rusakov DA, Fine A (2003) Extracellular Ca2+ depletion contributes to fast activity-dependent modulation of synaptic transmission in the brain. *Neuron* 37(2):287–297.
5. Henneberger C, Papouin T, Oliet SH, Rusakov DA (2010) Long-term potentiation depends on release of D-serine from astrocytes. *Nature* 463(7278):232–236.
6. Oertner TG, Sabatini BL, Nimchinsky EA, Svoboda K (2002) Facilitation at single synapses probed with optical quantal analysis. *Nat Neurosci* 5(7):657–664.
7. Scott R, Ruiz A, Henneberger C, Kullmann DM, Rusakov DA (2008) Analog modulation of mossy fiber transmission is uncoupled from changes in presynaptic Ca2+. *J Neurosci* 28(31):7765–7773.
8. Jensen JB, Lauckner JE (2006) Novel probes for G-protein-coupled receptor signaling. *J Neurosci* 26(42):10621–10622, discussion 10622.
9. Lauckner JE, Hille B, Mackie K (2005) The cannabinoid agonist WIN55,212-2 increases intracellular calcium via CB1 receptor coupling to Gq/11 G proteins. *Proc Natl Acad Sci USA* 102(52):19144–19149.

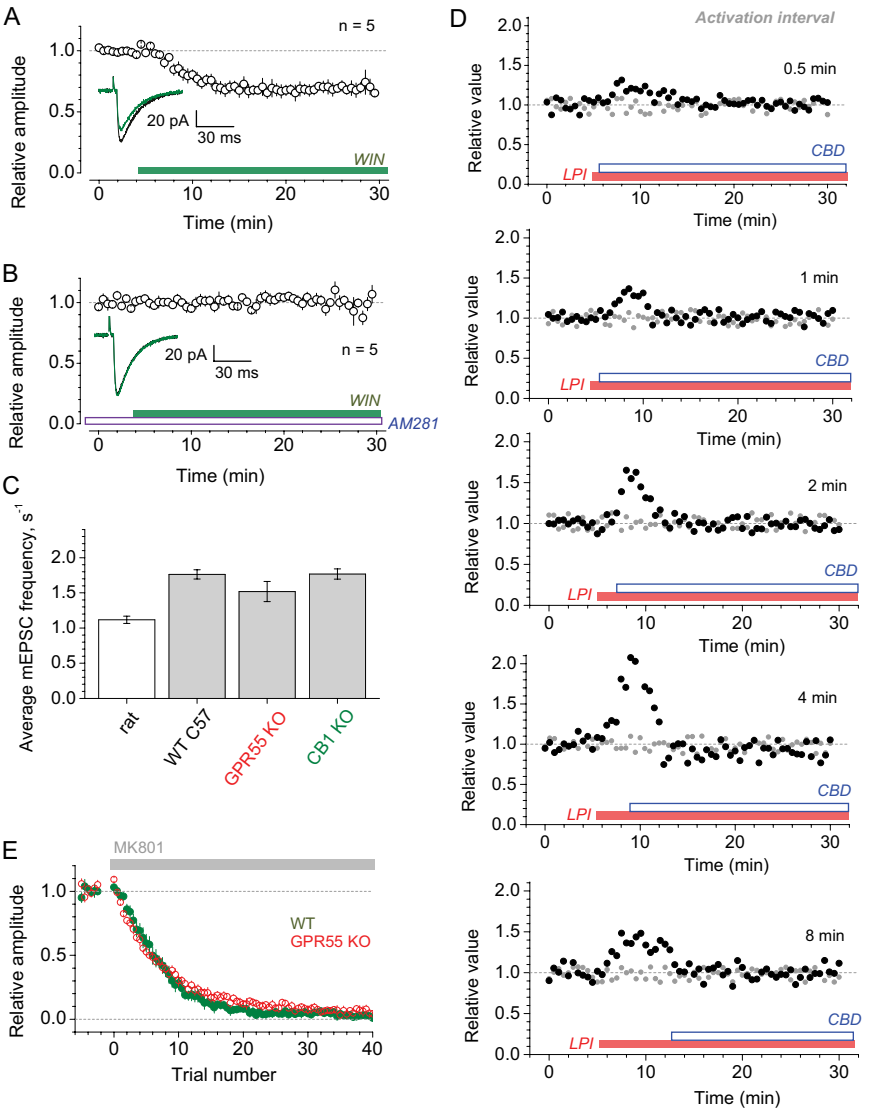

Fig. S1. Probing the role of cannabinoid-sensitive receptors on CA3-CA1 transmission. (*A*) The CB1 receptor agonist WIN55,212 (500 nM) inhibits CA3-CA1–evoked synaptic responses. Average time course of the amplitude (mean ± SEM, $n = 5$) of EPSCs evoked at CA3-CA1 synapses during application of WIN55,212, as indicated is shown (average inhibition 33 ± 4%, $n = 5$, $P < 0.002$). (*Inset*) One cell example: average responses in control (black) and 20–30 min after application (green). (*B*) One-hour preincubation with CB1 receptor antagonist AM281 (500 nM) abolishes the effect of WIN55,212 ($n = 5$). The other notation is as in *A*. (*C*) Average frequencies of mEPSCs recorded from CA1 pyramidal cells in the experimental species used. Bars, mean ± SEM values shown for rats (1.11 ± 0.05; $n = 35$), wild-type C57 mice (1.76 ± 0.06; $n = 17$), GPR55 knockout (1.52 ± 0.14, $n = 7$), and CB1 knockout (1.77 ± 0.07, $n = 5$), as indicated. (*D*) The time course of the facilitatory effect of GPR55 agonist LPI on spontaneous mEPSCs does not depend on the duration of agonist application. Plots show the frequency (black) and average amplitude (gray) of mEPSC, normalized to baseline during application of LPI (4 μM), and the subsequent blockade of GPR55 receptors by cannabidiol (CBD, 1 μM), at different time intervals between the drug applications (Activation interval), as indicated. The time course of the LPI-induced facilitation does not depend on the LPI exposure time, suggesting that it involves long-lasting downstream effects of receptor activation. (*E*) Average probabilities of evoked release at CA3-CA1 synapses are indistinguishable between the wild-type and GPR55 knockout animals. The graph shows the average EPSC decay time course in MK801 (mean ± SEM); the decay constants were 7.22 ± 0.14 in wild type (green; $n = 6$) and 6.93 ± 0.17 in GPR55 knockout (red; $n = 5$). $V_h = +40$ mV; AMPARs, mGluRs, glycine, and GABA receptors are blocked.

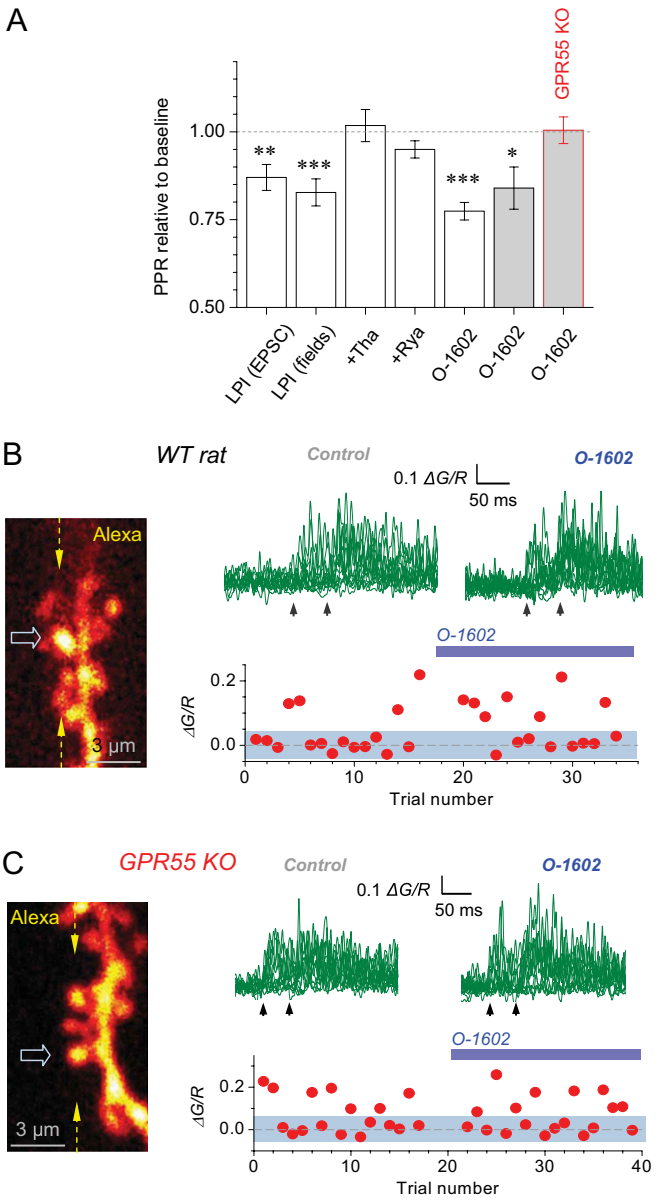

Fig. S2. Activation of GPR55 increases release probability of evoked postsynaptic responses at CA3-CA1 connections. (*A*) Paired-pulse facilitation values (mean ± SEM) averaged over the 2- to 7-min postapplication, relative to the baseline value averaged over ~5 min before the application onset. The paired-pulse ratio (PPR) is decreased following application of LPI (4 μM, by 13 ± 4% for field EPSPs, $n = 10$, $P < 0.007$; and by 17 ± 4% for whole-cell EPSCs, $n = 7$, $P < 0.005$), whereas the presence of thapsigargin (+Tha, 10 μM) or ryanodine (+Rya, 100 μM) abolishes the effect. The GPR55 agonist O-1602 decreases the PPR in rats (O-1602, white column; by 23 ± 3%, $n = 4$, $P < 0.003$) and in wild-type mice (O-1602, gray column; by 15 ± 6%, $n = 4$, $P < 0.04$), but not in the GPR55 knockout (GPR55 KO, red border, change 0.5 ± 3.8%, $n = 4$), as indicated. (*B*) The GPR55 agonist O-1602 increases release probability at individual CA3-CA1 synapses in the rat hippocampus: one-cell example of an optical quantal analysis. (*B Left*) The dendritic spine of interest (block arrow; dotted arrows, linescan position; Alexa channel, $\lambda_x^{2P} = 800$ nm; CA1 pyramidal cell held in whole-cell mode, as in Fig. 2). (*B Right Upper*) Time course of Ca^{2+} fluorescence evoked in the dendritic spine shown on the left by paired stimuli applied to Schaffer collaterals (interval 50 ms), before and after application of O-1602 (100 nM), as indicated; arrows, stimulus onsets. (*B Right Lower*) Δ*G*/*R* amplitudes of first Ca^{2+} responses in the same experiment; blue segment, the amplitude range counted as no response/failure (twice the SD of the baseline noise). (*C*) The GPR55 agonist O-1602 has no effect on release probability at individual CA3-CA1 synapses in the GPR55 knockout mice: one-cell example of an optical quantal analysis. The other notation is as in *B*.

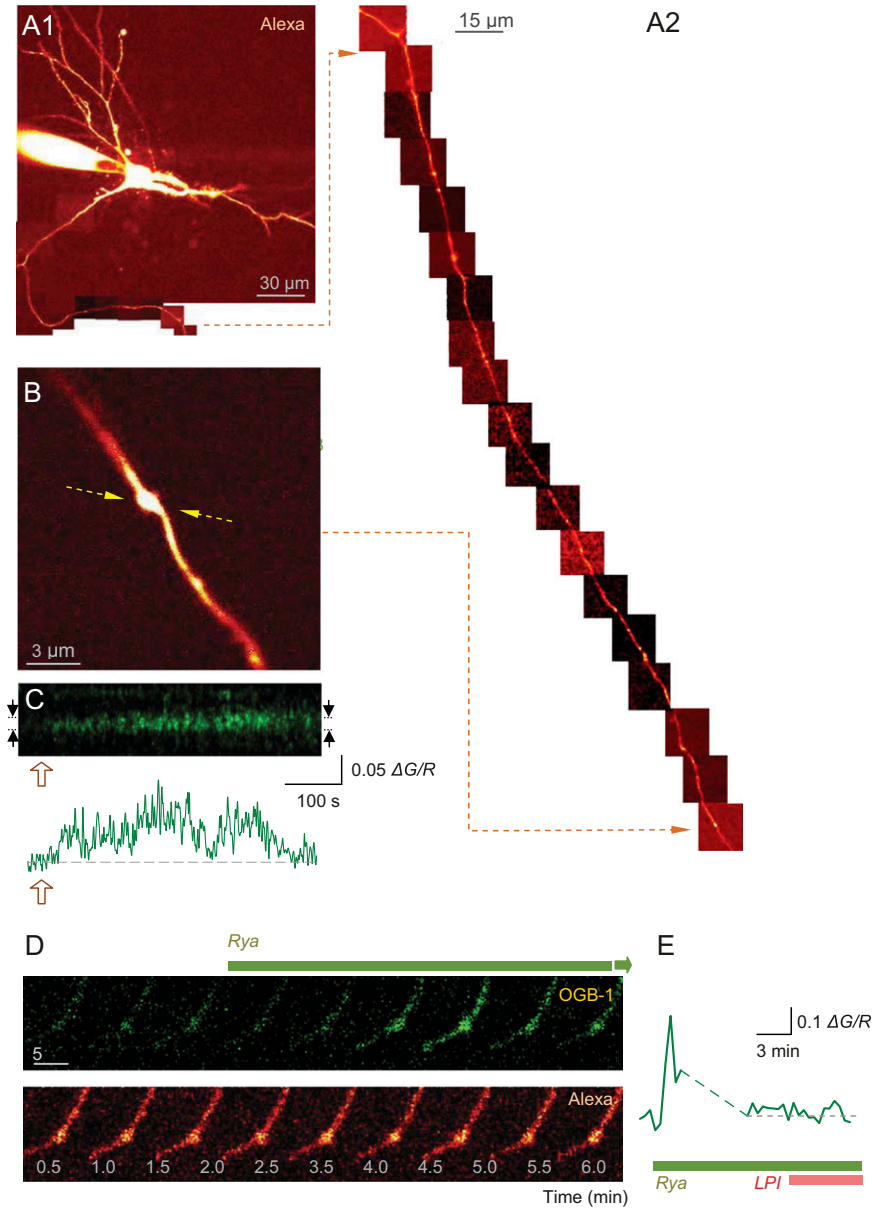

Fig. S3. GPR55 agonists trigger a prominent Ca^{2+} store-dependent Ca^{2+} elevation in presynaptic boutons of CA3-CA1 connections. (*A1* and *A2*) A characteristic experiment in which CA3 pyramidal cell with its axon traced into area CA1 from the cell soma using two-photon excitation microscopy (50 μM Alexa Fluor 594 channel); a collage of image z-stacks each Kalman averaged over a depth of 10–15 μm. (*B*) The axonal bouton of interest in area CA1 (Alexa channel), enlarged from the reconstructed image in *A2*, as indicated by the orange arrow; yellow arrows show linescan positioning. (*C Upper*) Linescan of Ca^{2+}-dependent fluorescence recorded from the bouton in *B* (Fluo-8 channel, rate one scan per second) reveals a prominent Ca^{2+} transient following application of O-1602 (block arrow). Black arrows and dotted lines, ROI for Ca^{2+} signal quantification. (*B Lower*) The corresponding $\Delta G/R$ trace representing the ratio of the Ca^{2+}-dependent signal in the "green" Fluo-8 channel to the signal in the "red" Alexa channel (with the subtracted photobleaching component). (*D*) One hundred micomolar ryanodine (final concentration) induces a prominent elevation in presynaptic Ca^{2+} in individual CA1 pyramidal cell axonal boutons, suppressing the effect of LPI applied subsequently: a single-bouton example. *D Upper* and *Lower* show frame scans in the green (OGB-1, Ca^{2+} indicator channel) and red (Alexa Fluor 594, morphology channel) channels, respectively; time points are shown. (*E*) The $\Delta G/R$ time course from the experiment shown in *D*; the time scale is extended beyond that on the images, as indicated. Note that when ryanodine is applied at a high concentration, the target cells inside the acute slice will be exposed to its levels gradually rising from zero to its maximal value.

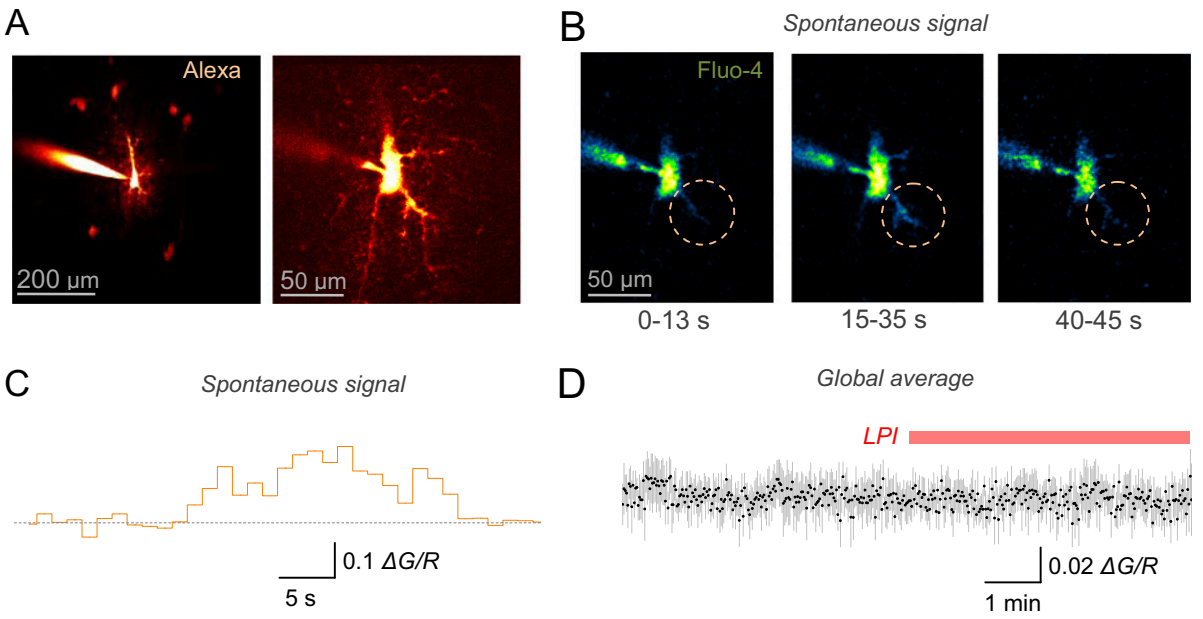

Fig. S4. GPR55 receptor agonist LPI has no effect on astroglial Ca^{2+}. (*A*) A passive CA1 astrocyte held in whole-cell mode (patch pipette is seen) shown as a 3D-stack average at lower magnification including gap-junction connected neighboring cells (*Left*) and a single optical section at higher magnification (*Right*; Alexa channel for Ca^{2+} imaging reference): one-cell example. (*B* and *C*) One-cell example: reliable detection of spontaneous Ca^{2+} signals in the astrocyte shown in *A* using time series frame capture (rate 0.75 Hz), images in *B* show frame averages over the time intervals as indicated (dotted circle, ROI), and trace in *C* shows frame-by-frame fluorescence signal recording (normalized over "red" Alexa signal *R*, $\Delta G/R$) within the ROI depicted in *B*. (*D*) Application of LPI induces no detectable Ca^{2+} astrocyte signal (ROIs routinely included the entire visible astrocytic tree but excluded the soma). Dots and gray bars, mean ± SEM of Ca^{2+} signal averaged across individual time-matched frames in $n = 6$ astrocytes.

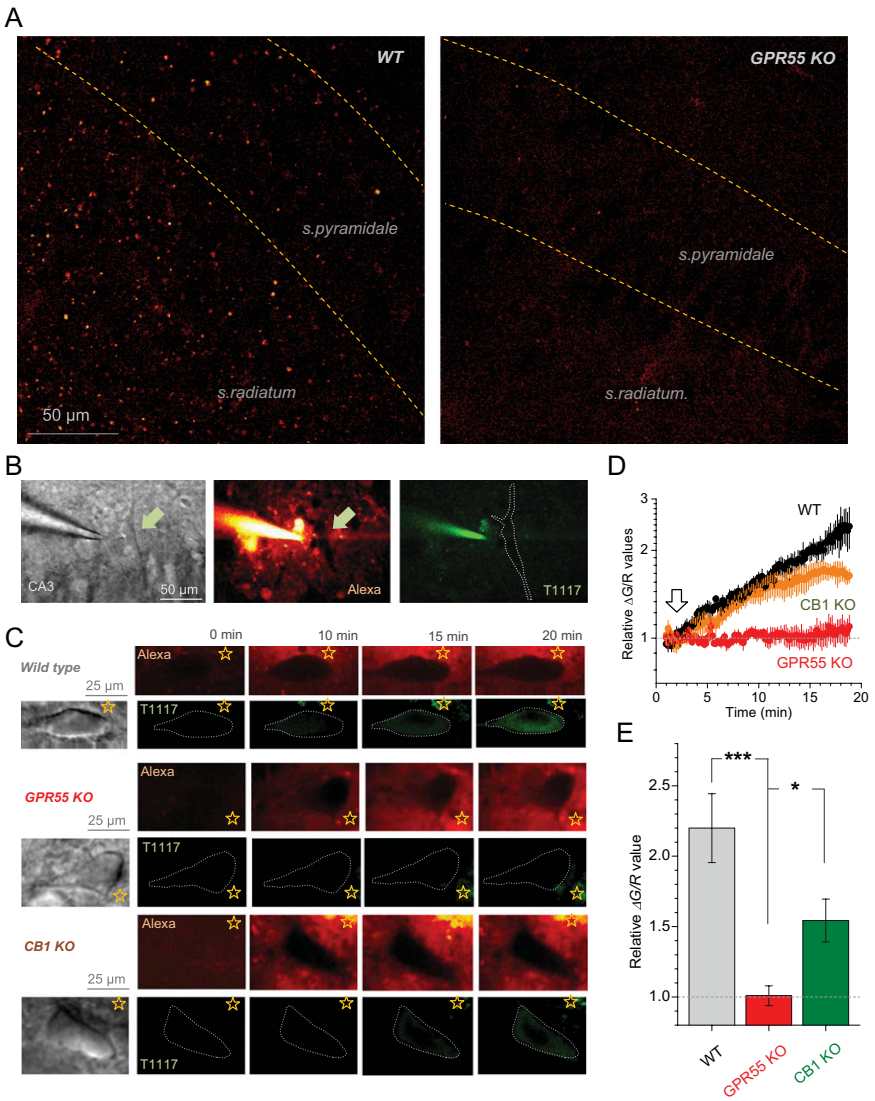

Fig. S5. Expression of GPR55 in hippocampal area CA1 and in presynaptic CA3 pyramidal cells: supporting data. (*A*) Characteristic fluorescence images of area CA1 labeled with Alexa-conjugated GPR55 antibody in wild-type (*Left*) and GPR55 knockout (*Right*) samples (λ_x = 488 nm), as indicated; images represent illustrations from Fig. 4*B* shown at higher resolution. (*B*) GPR55 staining of live cells with T1117 in acute slices: A pressurized pipette (~3 μm tip, filled with 0.3 μM T1117 and 20 μM Alexa Fluor 488) in bath solution is near the CA3 pyramid cell (block arrow; slightly outside the layer to maximize dye access). Pressure is applied for ~20 min, cells are monitored by using DIC (*Left*), Alexa (*Center*), and T1117 (*Right*) channels. In the Alexa channel, the cell body outline remains unstained, indicating little nonspecific uptake (*Methods*). (*C*) Snapshots of Alexa and T1117 fluorescence near CA3 pyramids during T1117 application (onset at ~3 min, time points shown) for three species, as indicated, in two channels; stars mark the position of the pressure pipette tip (local tissue damage near the tip may lead to local residual nonspecific staining in both channels). (*D*) The time course of T1117 versus Alexa fluorescence ($\Delta G/R$) in CA3 pyramids during pressure application in wild type (n = 5), CB1 KO (n = 3) and GPR55 KO (n = 6), as shown; arrow, application onset. (*E*) Statistical summary for the $\Delta G/R$ signal at 18–20 min relative to 4–5 min after pressure application onset; ***P < 0.001; *P < 0.025 (P = 0.12 for the difference between CB1 KO and wild-type).

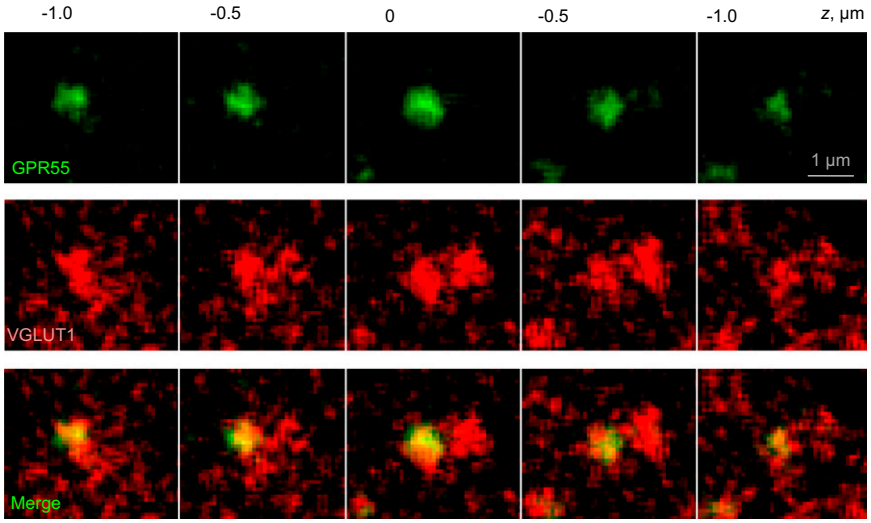

Fig. S6. Three-dimensional immunocolocalization of GPR55 and VGLUT1 in area CA1 at high magnification. An example stratum radiatum fragment showing individual tentative axonal boutons labeled with Alexa-conjugated GPR55 and VGLUT1 antibodies, shown in several serial confocal sections 0.5 μm apart, as indicated. The fragment represents a zoomed-in area from the sample shown in Fig. 4*E* containing two or three boutons, as seen. Clear distinction between GPR55 and VGLUT1 labeling patterns indicates negligible contaminant bleed-through signal.

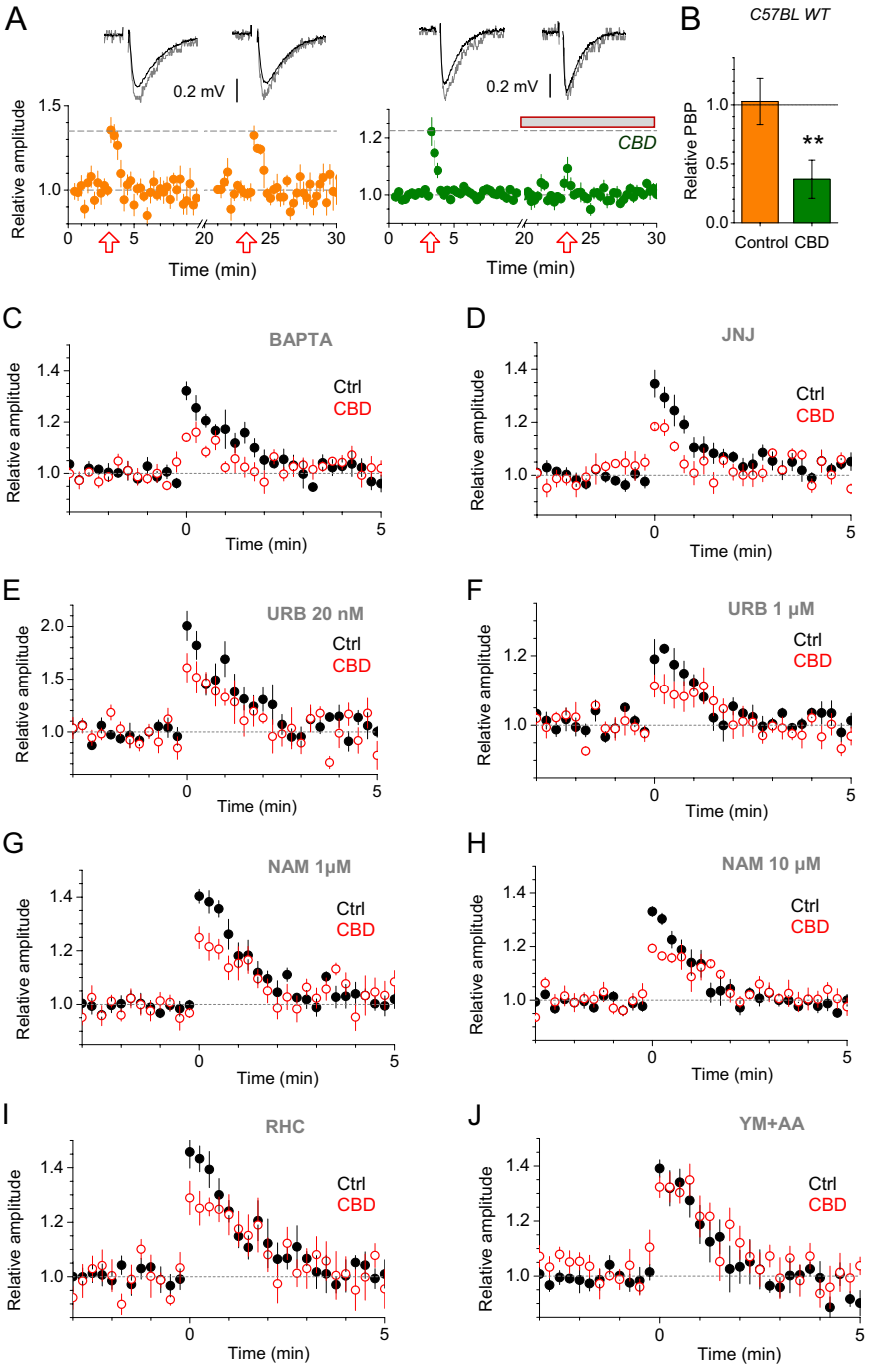

Fig. S7. Dissecting the contribution of GPR55-reated signaling to short-term PBP. (*A*) Blockade of GPR55 suppresses synaptic PBP in the wild-type mice. Average time course of PBP (monitored with fEPSPs evoked by stimulation of Schaffer collaterals) induced twice by a bursts of stimuli (10 pulses at 100 Hz, red block arrow) in control (*Left*, $n = 6$) and test (*Right*, $n = 7$) wild-type groups of mice; 1 μM CBD was applied after the first PBP in the test group, as indicated. Dots, fEPSP amplitude (proportional to the initial rise slope throughout) relative to baseline; error bars, SEM. Traces are characteristic examples of baseline (black, average of 10) and potentiated (gray, the first response after train) fEPSPs, correspondingly. (*B*) The average ratio "second-to-first PBP" in control and test (CBD) samples; average PBP values were calculated by using three fEPSPs after train. $^{**}P < 0.009$. (C) Average time course of PBP (mean ± SEM of the EPSC amplitude; spike burst corresponds to $t = 0$ on the plots) in baseline conditions (black circles, $n = 5$) and following application of 1 μM cannabidiol (red open circles, $n = 5$), with the high-affinity Ca^{2+} buffer BAPTA (100 mM in total) in the whole-cell recording pipette; two sequential epochs overlapped for direct comparison. (*D–J*) Experiments as in *C* but carried out following 1-h incubation with fatty acid amide hydrolase inhibitors JNJ 1661010 (100 nM JNJ in *D*, $n = 5$), URB-597 (0.02 and 1 μM URB in *E* and *F*, respectively, $n = 5$), monoacylglycerol lipase inhibitor *N*-arachidonyl maleimide (1 and 10 μM NAM in *G* and *H*, respectively, $n = 5$), diacylglycerol lipase inhibitor RHC 80267 (10 μM RHC in *I*, $n = 5$), and phospholipase A_2 inhibitors YM 26734 and AACOCF3 applied together (20 μM and 10 μM, respectively, YM+AA in *J*, $n = 5$). Synaptic responses were monitored with fEPSPs. See text and Fig. 5 for further details and statistical summaries.

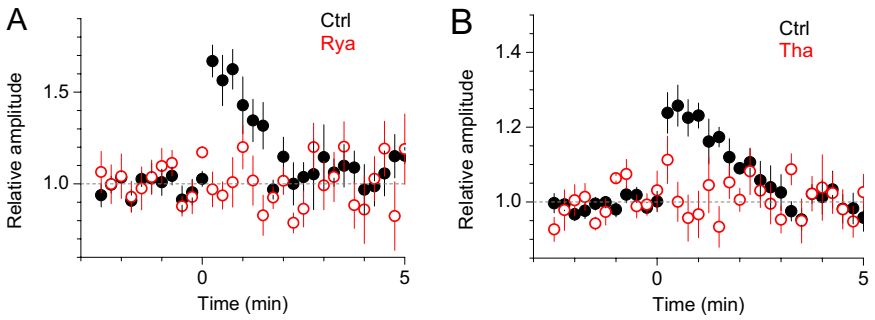

Fig. S8. Short-term PBP at CA3-CA1 synapses depends on Ca^{2+} stores. Average time course of PBP (mean ± SEM of the fEPSP amplitude) induced twice by 10 pulses at 100 Hz (at time 0) in baseline conditions (black circles) and after application of 100 μM ryanodine (Rya in *A*, $n = 5$) and 10 μM thapsigargin (Tha in *B*, $n = 5$). See text and Figs. 5 and 6 for further details and statistical summaries.